Geoderma 447 (2024) 116914

Contents lists available at ScienceDirect

Geoderma

journal homepage: www.elsevier.com/locate/geoderma

Assessment of different agricultural soil compaction levels using shallow seismic geophysical methods

Alberto Carrera [a,*], Ilaria Barone [b], Mirko Pavoni [b], Jacopo Boaga [b], Nicola Dal Ferro [a], Giorgio Cassiani [b], Francesco Morari [a]

[a] DAFNAE Department, University of Padova, 35020 Legnaro, Italy
[b] Geoscience Department, University of Padova, 35100 Padova, Italy

ARTICLE INFO

Handling editor: Haly Neely

Keywords:
Agrogeophysics
Seismic Refraction Tomography
MASW
Soil structure

ABSTRACT

A well-developed soil structure is crucial for a fertile soil and rules its influence on the ecosystem. Slight variations in the way soil components are organized and connected can greatly impact the soil mechanical and hydraulic characteristics. However, these features are challenging to measure at a scale that is relevant for agricultural management. In this study, we assess the capability of two seismic geophysical methods, i.e. Seismic Refraction Tomography and Multichannel Analysis of Surface Waves, to monitor the effects of compaction on agricultural bare soil. The purpose is to highlight the different mechanical response caused both by soil plastic deformation and soil water distribution due to increasing compaction. Results demonstrate that both geophysical techniques provide sufficient information to capture the effects of soil compaction and distinguish its significance, while traditional direct measurements, being punctual, lack sufficient spatial coverage. P-wave velocities carry a strong imprint of soil compaction, provided by seismic refraction, incorporating the information given by the multiphase medium in its entirety. On the other hand, S-wave velocity derived from Surface Waves discriminates the effect of solid matrix structure. This work, moreover, aims to pave the way for seismic methods to spatially characterize compaction at field scale, illustrating its potential and suggesting possible developments.

1. Introduction

Soil structure is the spatial arrangement of solid constituents and voids (Dexter, 1988), and reflects natural biotic (i.e. soil fauna and roots) and abiotic factors (e.g., sedimentation, freezing-thawing and wetting–drying), as well as human activities through soil tillage, organic matter addition and crop management. Soil compaction is one of the most impactful drivers of soil structure degradation, leading to densification and distortion of the soil spatial arrangement due to the breakdown of soil aggregates under loads that exceed the soil's inherent stability (Schjønning et al., 2019).

Soil compaction due to traffic with modern agricultural machinery has dramatically increased (Gürsoy, 2021; Keller et al., 2019; Raper, 2005), causing significant impacts on soil ecosystem services, in particular regulating and production services (e.g., flood control, agricultural production), resulting in significant ecological threats to biodiversity and economic damage to farmers and society (Bronick and Lal, 2004; Hamza and Anderson, 2005; Nawaz et al., 2012).

Quantification of soil structure and soil compaction has been traditionally conducted through direct measurements of dry bulk density and porosity, or inferential measurements that rely on either increase in soil strength (e.g., soil penetration resistance) or reduction in interconnected pore spaces (e.g., air and water permeability) (Johnson and Bailey, 2002; Keller et al., 2021b). Regardless of whether they are conducted in-situ or in a laboratory after sampling, these methods are limited in their ability to quantify soil structure dynamics – including compaction – over space and time. Soil compaction phenomena exhibit highly spatially and temporally variability, depending on factors such as intensity and distribution of the traffic of agricultural machineries and/or the implementation of tillage practices (Alaoui and Diserens, 2018), which dominate over the nonetheless present natural processes (Fabiola et al., 2003).

Several geophysical techniques, as outlined by Romero-Ruiz et al. (2018), can complement traditional characterization methodologies. With the advantage of their non-invasive nature, these techniques can be readily applied to various spatial and temporal scales. The most

* Corresponding author.
E-mail address: alberto.carrera@phd.unipd.it (A. Carrera).

https://doi.org/10.1016/j.geoderma.2024.116914
Received 13 July 2023; Received in revised form 1 May 2024; Accepted 8 May 2024
Available online 21 May 2024

widespread methods for soil investigations rely on the distinct electrical properties of soils determined by soil texture (mainly clay content) and organic matter content, and changes in volumetric content and salinity of pore fluids. Electrical and electromagnetic techniques are very often used in the characterization of soil properties such as bulk density, gravel and clay content (Morari et al., 2009) as well as state variables like soil salinity and water content (Blanchy et al., 2020; Carrera et al., 2022; Cassiani et al., 2015; Doolittle and Brevik, 2014; Hanssens et al., 2019), and even characterize the variability of soil compaction (Islam et al., 2014a, 2014b). Recent works have also studied the phenomenon of compaction with geoelectrical methods both in the laboratory (Seladji et al., 2010) and on a field scale (Besson et al., 2013; Romero-Ruiz et al., 2022). In addition, other studies tried to identify reflections of electromagnetic waves from soil compacted layers and lateral continuity of shallow horizons using Ground Penetrating Radar (Jonard et al., 2013; Muñiz et al., 2016; Zajícová and Chuman, 2019). However, the electromagnetic response of soil is influenced by a number of factors (mineralogy, texture, porosity, fluids, organic matter), highlighting the complexity inherent in understanding which factor is predominant in a site-specific situation. Active seismic methods have been widely employed for large scale crustal studies (Cho et al., 2006; Zelt et al., 2003), mineral resources exploration (Darijani et al., 2020; Wright, 1981), engineering and geotechnical characterization at smaller scale (Boaga et al., 2011, 2021; Foti et al., 2011), slope stability and land management (Barone et al., 2021; Samyn et al., 2012; Uhlemann et al., 2016a). However, the application of seismic methods in agricultural science remains relatively unexplored, despite their potential to provide unique insights into the mechanical properties of materials. The pedosphere, being subject to deformation and changes in dry bulk density, exhibits corresponding variations in seismic waves velocities. Thus, seismic investigations can contribute to assessing soil structure changes and compaction phenomena in both the tilled topsoil layer and the untilled subsoil profile beneath.

Interesting studies in this direction have been proposed by Keller et al. (2013) and Romero-Ruiz et al. (2021) to link the soil strength to compressional (P) wave velocity, and by Donohue et al. (2013) to explore the use of surface waves to evaluate soil compaction. Blazevic et al. (2020) emphasized the usefulness of seismic-electrical tomography for monitoring hydrological processes in unsaturated soils, while Uyanik (2010) showed pioneering information on experimental precautions to be taken when measuring compression and shear waves in unconsolidated top-soils. Given the complexity of seismic response in partially saturated and unconsolidated soils, laboratory experiments remain essential (Pasquet et al., 2016).

Moreover, the use of these methods as monitoring over time could become crucial for the study of other soil dynamics, such as wetting–drying cycles (Fomin et al., 2023) and shrinking processes (Coppola et al., 2012), allowing a characterization directly in the field.

In this work, we propose the application of active seismic methods to retrieve information about changes in the soil structure as affected by compaction. Among the different techniques, we applied the Seismic Refraction Tomography (SRT) and the Multichannel Analysis of Surface Waves (MASW) to the same survey dataset, in order to retrieve the body (P and S) wave velocity profiles in a test site. The first technique has been used to obtain the compressional (P) waves velocities, and the latter to calculate the shear (S) waves velocities. The geophysical results have been compared with information derived from direct soil analysis (i.e. laboratory analysis on collected samples and penetration resistance measurements).

The objectives of this study are to (a) contribute in the adaptation process of the seismic geophysical techniques, commonly used in geosciences and engineering, to shallow soil science applications; (b) test the sensitivity of SRT and MASW in identifying soil structure variability along a soil profile in a well-controlled compaction experiment; (c) explore potential future applications of agrogeophysical studies in understanding the soil response to compaction, including its mechanical properties, plastic deformation, and water distribution.

2. Theoretical background

Active seismic methods rely on the introduction of mechanical energy into the subsurface through either an impulsive source, such as a sledgehammer, a weight-drop, or an explosive, or a vibrating source, such as a vibroseis. The propagation of this energy is measured at various distances, typically using geophones (Everett, 2011; Kearey and Brooks, 2002). A seismic source generates several types of seismic wave types, including body waves (compressional P-waves and shear S-waves), which can propagate through the medium (in our case, the soil), and surface waves (Rayleigh waves and Love waves), which are guided along the free surface of the medium, such as the soil-air interface in our case (Telford et al., 1990).

2.1. Body waves

According to the "perfect elasticity" assumption (Pelissier, 2007), P- and S-waves exist as solutions of the wave equation (Fleisch and Kinnaman, 2015).

As compressional waves propagate by uniaxial strains, and shear waves by shear strain, the velocities of P-waves (V_p) and S-waves (V_s) (m s^{-1}) in a homogeneous elastic medium are given by:

$$V_p = \sqrt{\frac{k + 4G/3}{\rho}} = \sqrt{\frac{(1-\nu)E}{(1+\nu)(1-2\nu)\rho}} \quad (1)$$

$$V_s = \sqrt{\frac{G}{\rho}} = \sqrt{\frac{E}{2\rho(1+\nu)}} \quad (2)$$

Where k (Pa) and G (Pa) are the bulk and shear elastic moduli, ρ (kg m^{-3}) is the bulk density of the medium, E *(Pa)* is the Young's modulus and ν is the Poisson's ratio. The Young's modulus E (Pa) is a ratio of the longitudinal stress to the longitudinal strain with no lateral constraint. Low values tend to indicate ductile or soft materials, high values brittle or stiff materials (Ma et al., 2016). The shear modulus G (Pa), also known as modulus of rigidity, expresses the elastic body's response in terms of shear strain to a given applied shear stress. Shear strength and shear modulus are proportional in cohesive soil (Hara et al., 1974; Uhlemann et al., 2016b). The bulk modulus k (Pa) describes the volume change of an elastic material in case of variations in the hydrostatic pressure.

Equations (1) and (2) form the basis for the use of seismic waves in material characterization. While soils are generally categorized as inelastic materials, they can exhibit linear elastic behaviour within a very small deformation range triggered by the passage of mechanical waves. This behaviour is observed when the deformations remain sufficiently small to prevent any sliding of the grain contacts (Ammon et al., 2021; Telford et al., 1990).

Note that while V_p is a characteristic of the entire medium, including both the solid matrix and fluids in the pore space, V_s is only associated with the solid matrix. V_s reflect density variations and/or rearrangement of sediments, since pore fluids do not respond to shear stresses. Despite that, it has been observed that the shear modulus is sensitive to capillary forces (linked with water content) at shallow depths (Romero-Ruiz et al., 2021; Shin et al., 2016; Solazzi et al., 2021).

2.2. Rayleigh waves

Rayleigh waves are a type of surface waves that travel along the earth-air interface causing an elliptical soil motion (for an exhaustive treatment see Aki and Richards (1980) and Rayleigh (1885)). This characteristic allows for their detection using also conventional single-component (vertical) geophones. The use of Rayleigh waves to

determine the elastic properties of the subsurface is based on their dispersive behavior in vertically heterogeneous media (Thomson, 1950). Lower frequency (longer wavelength) waves exhibit greater sensitivity to the elastic properties of deeper (and usually faster) materials, while higher frequency (shorter wavelength) waves are more sensitive to shallower (and usually slower) materials.

The velocity of individual phases within a Rayleigh wave train is referred as phase velocity. To infer the relationship between phase velocity and frequency (or wavelength), a spectral analysis of Rayleigh waves is conducted, also known as dispersion curve (Xia et al., 1999). Multiple phase velocities can coexist for a given frequency, and this modal behavior is represented by an infinite number of dispersion curves (i.e. modes), each corresponding to independently propagating dispersive Rayleigh wave packets (Tselentis and Delis, 1998). The mode exhibiting the lowest phase velocity is termed the fundamental mode. Higher modes are characterized by higher phase velocities and provide information about deeper layers, however they exist only above a specific cut-off frequency (Tokimatsu et al., 1992).

As phase velocity of Rayleigh surface wave (V_r) is strongly related, through Poisson's ratio, with the S-wave velocity V_s ($0.87V_s < V_r < 0.96V_s$) (Richart, 1970), dispersion curves are then subjected to geophysical inversion in order to produce V_s depth profiles consistent with the data (Foti et al., 2014). Note that this inversion procedure, in general, is limited to 1D modelling with depth, and assumes lateral homogeneity, which may not always true in reality (Barone et al., 2023, 2022; Vignoli et al., 2016, 2011; Vignoli and Cassiani, 2010).

3. Material and methods

3.1. Site description

The experiment was conducted at the Experimental Farm "L. Toniolo" of the University of Padova in Legnaro (45°21′ N; 11°57′ E, 8 m a.s.l.), North-Eastern Italy (Fig. 1a). In the study area, the soil is classified as Fluvi-Calcaric Cambisol (WRB, I.W.G., 2014) which represents almost 50 % of the Venetian plain in the Veneto region. It is a poorly layered silt-loam soil with low natural fertility due to a small organic carbon content (about 0.8–1 % at the 0–20 cm layer, down to 0.05 % at 60–90 cm) and low cation exchange capacity (<20 cmol kg^{-1}) (Longo et al., 2021; Mencaroni et al., 2023).

The experiment was carried out in late Spring 2022 (18th May) on 6 bare soil plots, 1 m wide and 15 m long each and spaced 2 m apart, in a total 400-m^2 area (Fig. 1b). We selected the most homogeneous field area based on previously collected information through Frequency-Domain Electromagnetic Method (FDEM) mapping (CMD Mini-explorer, GF Instruments, CZ) and some previous historical information provided by the L. Toniolo farm staff (data not shown). Before the start of the experiment, the field was used for arable cropping following conventional agricultural practices, which involved moldboard ploughing down to 0.3 m depth and disk harrowing before seeding. For the specific experiment setup, the soil was tilled as previously described in late winter/early spring period (February-March 2022).

Two different degrees of topsoil compaction were experimentally recreated and compared against uncompacted conditions with two replications in a randomized design. The uncompacted plots (no compaction, hereafter called "NC") were treated without any machinery traffic, considering observations from these treatments as indicative of natural soil structure recovery in the absence of vegetation as reported in Keller et al. (2018) and Keller et al. (2021). A light-compaction (LC) treatment was obtained with traffic of a Fiat 680H tractor of 2940 kg weight (front: 1060 kg, rear: 1880 kg), while heavy-compaction (HC) was generated with a traffic of New Holland T7.165 S tractor of 9750 kg weight (front: 3580 kg, rear: 6110 kg). Each compaction event was performed with a double tractor pass, using a single-side wheeling as the

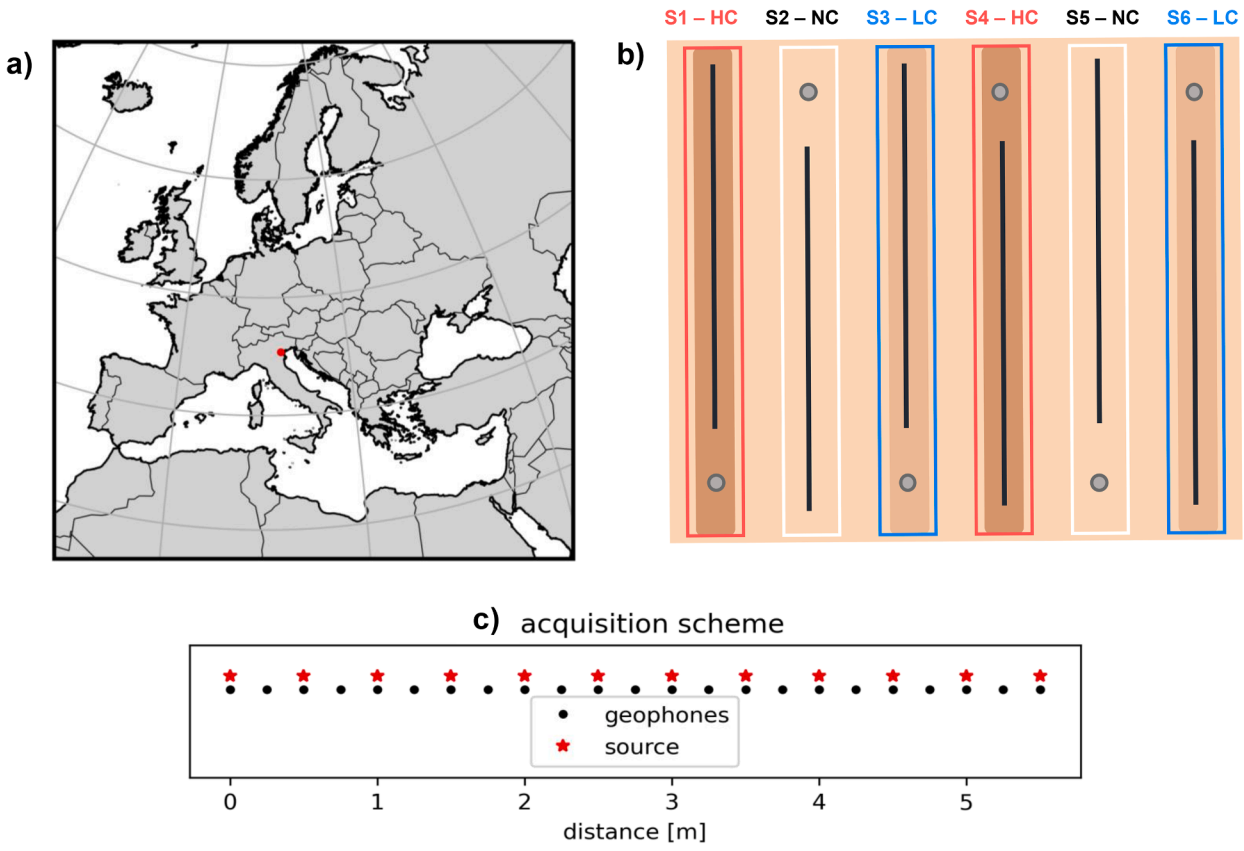

Fig. 1.

compaction strip within the elementary plots (see illustration in Fig. 1b). To maintain bare soil conditions, any emergent vegetation was suppressed through periodic application of nonselective herbicides (i.e. glyphosate).

A day after the compaction event, undisturbed soil samples of 7.2 cm diameter were collected down to 1 m at the head of each plot (six in total) using a hydraulic sampler and analyzed every 10 cm. Undisturbed soil samples were weighed, and a fraction (two-thirds) was oven-dried at 105 °C for 24 h for the calculation of the gravimetric water content and bulk density (BD). The other soil fraction (one-third) was air-dried and sieved through a 2-mm for texture analyses (soil skeleton was absent). Soil bulk density was estimated by the core method (Grossman and Reinsch, 2018) while soil texture was determined by laser diffraction (Mastersizer 2000; Malvern Panalytical Ltd, Malvern, UK) as described in Bittelli et al. (2019). Penetration resistance (PR) was measured with a penetrologger (Eijkelkamp, Netherland), throughout the 0–80 cm layer, with a 30° 2 cm^2 cone. In each plot, three PR sampling zones were randomly selected, for a total of 18 in-depth profiles.

Finally, along the centerline of each plot, active seismic surveys (black lines in Fig. 1b) were performed using both SRT and MASW approaches. The seismic source was moved to different positions along the geophones (i.e. signal transducers) array (respectively red stars and black dots in Fig. 1c). The acquisition scheme and parameters adopted for each survey line are further described in Section 3.2.

3.2. Seismic refraction Tomography (SRT)

The SRT method consists in the measurement of the first-arrival times of artificially generated body waves at given locations. All wave phenomena follow Snell's law and are subject to refraction and reflection at interfaces between materials with contrasting propagation velocities (Born et al., 1959). In refraction investigations, as the name implies, only refracted waves are considered. One of the main conditions for applying the method is that, in general, the propagation velocity of seismic waves increases with depth. To analyze the compressional (P) waves, vertical geophones are used, while horizontal geophones are

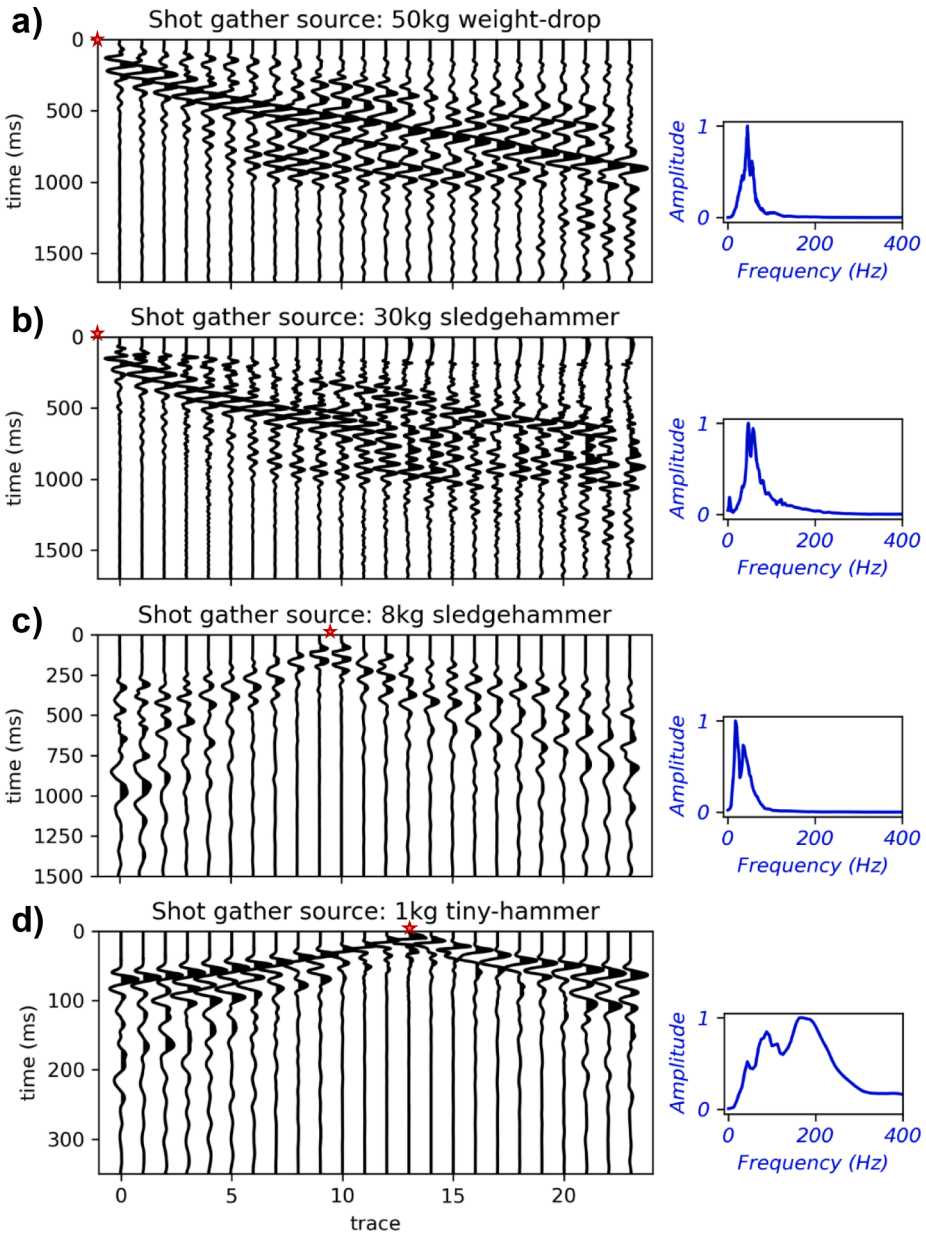

Fig. 2.

necessary for shear (S) waves. Since generating compressional waves is easier than shear waves, P-wave SRT approach is the most commonly adopted. Typically, several shot gathers (i.e. collection of seismic traces sharing common geometry) are recorded for different seismic source locations inside and outside the survey line. Iterative tomographic inversion procedure, involving raytracing, is used to obtain a 2D velocity model of the subsurface (Lehmann, 2007; Moser, 1991; White, 1989; Woodward, 1992; Moser and Nolet, 1992).

Common P-wave SRT surveys utilize sources that generate signals with dominant "low" frequencies (20–60 Hz – e.g., heavy hammers, free-falling mass, accelerated mass, and seismic guns). In this way, relatively large wavelengths (10 s – 100 s of meters – see Fig. 2a-c) are produced and, with an adequate length of the geophone array, it is possible to achieve large penetration depth. In our experiment, the target is the soil profile (ideally, down to 1–2 m) whose structure can be affected by mechanical stress causing compaction. Preliminary tests were carried out to determine the best source and receiver types and geometries capable of energizing and detecting sufficiently high frequencies, so that small wavelengths could sample the shallowest portion of the soil (i.e. down to 1.5–2 m). Therefore, a small-scale and high-resolution array has been settled with 24 vertical geophones spaced 0.25 m, with a natural frequency of 100 Hz, and a very light seismic source has been chosen (1 kg hammer striking a 10 cm^2 slender stainless-steel plate). As can be seen in Fig. 2, the excited frequencies during the experiment ranged between 20 and over 400 Hz (Fig. 2d), while in P-wave SRT surveys performed with conventional seismic sources and

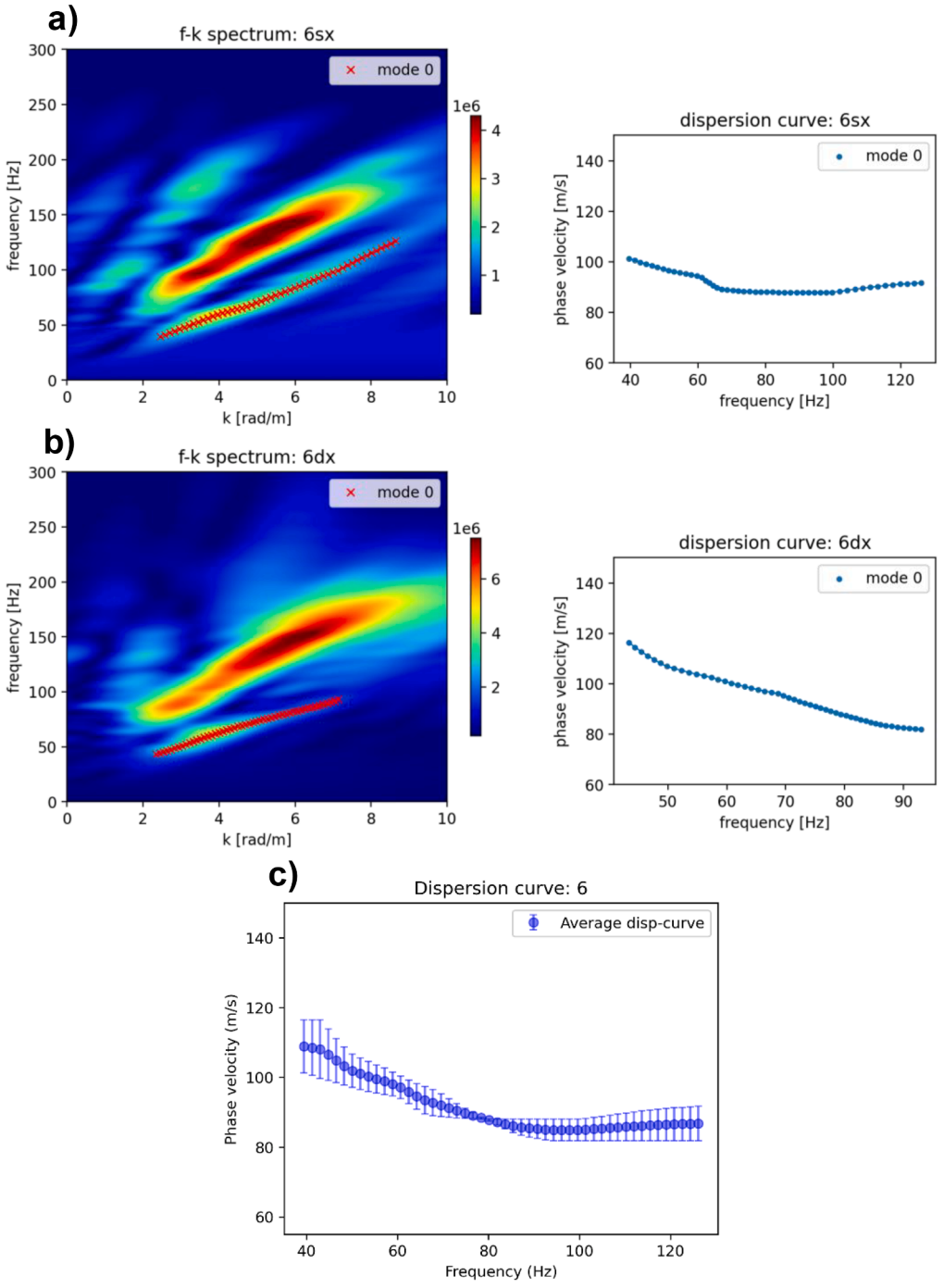

Fig. 3.

geophones, and with larger receiver spacing, this range is typically much lower (0–150 Hz, Fig. 2a-c).

Surveys were collected using a Geode seismograph (Geonics, USA), acquisition scheme and profile locations can be found in Fig. 1c. In each dataset of the experiment, the signal-to-noise ratio remained high even at larger offsets, therefore no stacking procedure was applied on the seismic traces to attenuate noise. The picked first arrivals were inverted through the C++/Python-based library pyGIMLi (Rücker et al., 2017), discretizing the subsoil model with an unstructured triangular mesh. PyGIMLi utilizes a shortest path algorithm (Moser, 1991; White, 1989) which models seismic energy propagation as ray. We performed an L-curve analysis (Hansen, 2000) of the entire dataset acquired to define the most appropriate value of the regularization and smoothing parameters to be used in the inversion process (Wagner and Uhlemann, 2021). We also considered an absolute data error of 3 ms for inversion of the seismic data (around 10 %), that appears realistic since the seismogram traces were generally very clean. All inversions were conducted at 4:1 preferential horizontal smoothing. The models were updated by solving a regularized linear inverse problem. The ray-tracing steps were iterated until a satisfactory fit to the data was achieved, evaluating the model response with the dimensionless error-weighted χ^2 criterion. All our inversions ended with $1.04 < \chi^2 < 1.89$ (Fig. 5), falling within the range 1–5 defined by Günther et al. (2006) for reliable results, avoiding data overfit or underfit.

3.3. Multichannel analysis of surface waves

The Multichannel Analysis of Surface Waves (MASW) method (Park et al., 1999) uses multichannel systems to record the propagation of Rayleigh waves at different locations. The use of multiple geophones allows the simultaneous recording of a variety of wavelengths, thus each shot gather is analyzed in the frequency-wavenumber (f-k) domain, where the dispersion curve is defined by picking the maximum amplitudes associated with the different modes. Fig. 3 a-b shows as an example the analysis for the external shots of the survey on plot 6 (low-compaction LC).

Although the higher modes are very energetic and rather clear for nearly all the shot gathers analyzed, they were not included in the final analysis. Higher modes correct identification is indeed complex, especially when energy is distributed over them (Boaga et al., 2013, 2014; Zhang and Chan, 2003). If the higher modes are not properly identified, the obtained models may not represent the real subsoil. Therefore, although a forward model was created to guide the picking of the acquired data, to avoid the errors associated with the modal numbering, we only inverted for the fundamental mode. Note that the presence of energetic higher modes is not a surprise given the strong elastic impedance contrasts, and possible velocity inversions, as discussed later on.

For each survey line, the two external (i.e. the most right and the most left) shots were used to derive an average V_s profile. The left and right dispersion curves obtained were averaged, and their standard deviation was computed as an estimate of the picking error (Fig. 3c).

As for the inversion, the soil profile model was discretized in 3 layers with parametrization reported in Table 1. The choice was performed based on the information obtained from SRT and laboratory analysis on the extracted samples for each station.

Table 1
Subsoil model parametrization for dispersion curve inversion.

	Thickness range (m)	Vp range (m/s)	Vs range (m/s)	Poisson's ratio	Bulk density (kg m^{-3})
Layer 1	0.10–0.30	80–350	40–140	0.20–0.40	1200–1500
Layer 2	0.60–1.0	200–400	80–160	0.20–0.40	1200–1500
Layer 3	0.60–infinite	250–600	100–240	0.20–0.40	1600

The inversion was performed using the evodcinv Python library (Luu, 2021a), which adopts Evolutionary Algorithms for the optimization problem, in order to obtain the S-wave velocity profile as a function of depth. This is typically done by iteratively updating the initial model of the subsurface structure until the observed dispersion curve and the modeled dispersion curve match. In our case, we set 500 iterations for each inversion, using a Competitive Particle Swarm Optimization (CPSO) method (Luu, 2021b) with a total population size of 10, resulting in a misfit of the models averaging to less than 6.5 %. Since the obtained V_s models are composed of layers of varying thickness, they were resampled every 0.1 m with the mean value so as to be compared with the other variables in equal intervals.

3.4. Statistical analysis

The experimental design included 3 treatments (i.e. HC, LC, NC), 2 replicates per treatment, and 10 depths per replicate. Soil bulk density (BD), S-waves (V_s), soil water content (both gravimetric and volumetric), and penetration resistance (PR) were analyzed with a linear mixed-effect model considering soil depth and compaction treatment as categorical factors, and clay content as continuous factor. The P-waves (V_p) were analyzed with a linear mixed-effect model with the same categorical factors, but the gravimetric water content was included as continuous factor. Single effects and interaction between categorical factors were tested. Variability associated with the modelled means was provided by the Tukey's HSD (honestly significant difference) test at the 5 % level of significance.

Relationships between soil parameters and seismic results obtained at different depths were investigated through a correlation matrix by estimating Pearson's correlation coefficients. All depths when data were simultaneously collected were considered (n = 60 total observations per parameter). A backward stepwise multiple linear regression analysis was finally performed to identify the contribution of soil parameters, seismic measures and penetration resistance in explaining the variability of soil bulk density. The statistical analysis was performed using a Python script based on SciPy (Virtanen et al., 2020) and Statistica (StatSoft Inc., Tulsa, OK, USA).

4. Results

4.1. Soil measurements

Experimental machinery traffic has determined significantly different soil bulk density values ($p < 0.05$) among the treatments in the upper soil layers (0—–0.20 m). The LC and HC treatments exhibited higher BD with average values of 1.36 g cm^{-3} and 1.53 g cm^{-3}, respectively, compared to the NC that averaged 1.31 g cm^{-3} (Fig. 4a). In the 0.30—–1.0 m profile, the HC treatment presented BD values within the range of 1.46—–1.58 g cm^{-3}, while both the LC and NC treatments showed slightly higher values, respectively from 1.41 to 1.58 g cm^{-3} and from 1.36 to 1.50 g cm^{-3}.

Moisture content did not show significant differences in all the treatments (Fig. 4b-4c). However, there were notable changes in their distribution along the soil profile. Both GWC and VWC change significantly from 0.50 m depth and in subsequent layers compared to the 0—–0.40 m profile, with average values in depth (0.50 – 1.0 m) of 0.14 kg kg^{-1} (GWC) and 0.20 m3/m^{-3}(−|-) (VWC), whereas at 0—–0.40 m depth range the averages are 0.22 kg kg^{-1} (GWC) and 0.33 m3/m^{-3}(−|-) (VWC).

In terms of penetration resistance, compacted plots exhibited higher strengths compared to the non-compacted for the top 0.30 m depth (Fig. 4d). Down to a depth of 0.30 m, the average penetration resistance for the non-compacted soil was 0.32 MPa while showing higher values to an average of 0.81 MPa in LC and 1.20 MPa in HC. Even at greater

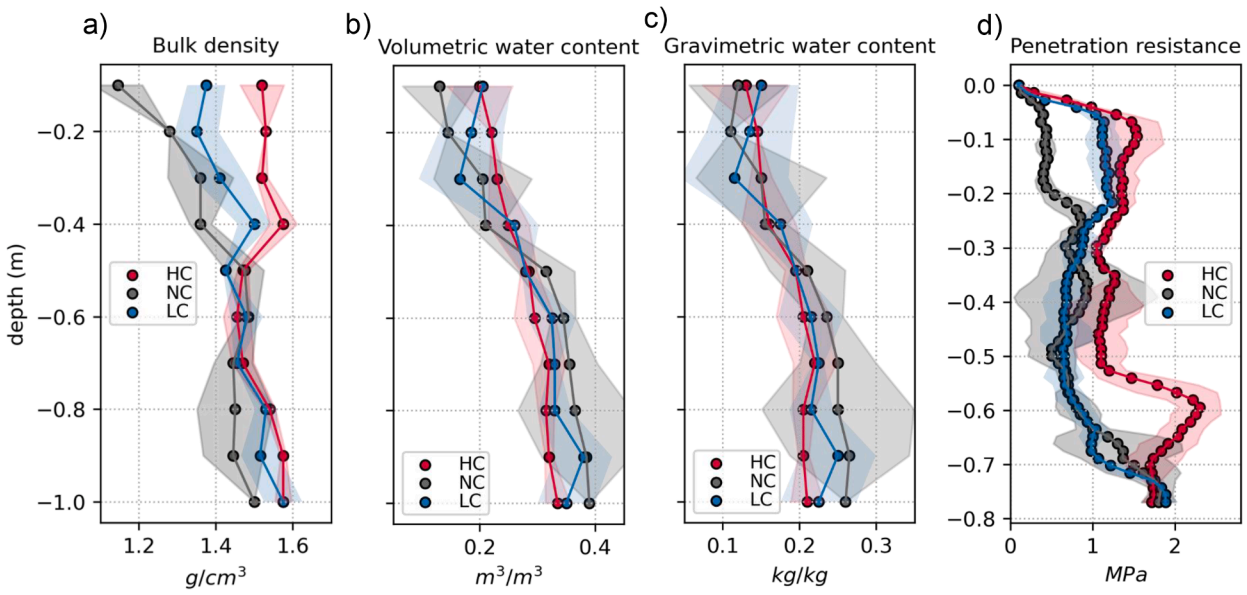

Fig. 4.

depths, beyond 0.40 m, HC consistently showed significantly greater values: its average value is more than 0.54 MPa higher than LC and 0.63 higher than NC, peaking at over 2 MPa at a depth of 0.60 m.

4.2. Seismic refraction Tomography

Fig. 5a shows the variation of the inverted P-velocity tomograms at increasing compaction level (downward) in the two different replicas (left and right). Note that the blanked areas within the sections are due to the absence of ray propagation within the mesh elements and therefore the corresponding areas are unreliable in terms of estimated wave velocities.

The seismic sections are very similar within the same compaction treatment. A general trend of increasing velocities with depth was evident for all models, exceeding 600 m s^{-1} from a depth of 1.30 m. Note however that SRT inherently tends to favor increasing velocity profiles with depth, unlike surface wave methods. The upper part (down to 0.50 m depth), exhibited the most significant variations among the different levels of compaction, with velocities ranging from 100 to 400 m s^{-1}. While average V_p of 185 m s^{-1} were found in the uncompacted soil, from the ground level down to a depth of approximately 0.4 m, the HC models averaged 245 m s^{-1},showing portions with $V_p > 250$ m s^{-1} right from the surface (0—–0.25 m depth). In the same 0—–0.40 m profile, light-compacted soil averaged 220 m s^{-1}, placing it almost in the middle compared with previous. Furthermore, even within the depth range of 0.50 m to 1.0 m, distinct velocity structure was observed between compacted (445 m s^{-1}, on average) and uncompacted (395 m s^{-1}, on average) soil, with localized areas exceeding 400 m s^{-1} found in the HC treatment.

Average 1D profiles of the two-dimensional tomographic models were computed to relate them to the other measurements (Fig. 5b). Based on V_p profiles, the velocities increased almost linearly with depth for all three treatments. They appeared shifted by a few tens of m s^{-1} according to the degree of compaction.

To better appreciate the differences between the models, which is not immediately possible by looking at the tomograms, we computed all possible combinations of the inversion normalizations with respect to NC. To highlight the sensitivity of the results to changes in compaction, Fig. 6 shows the ratios that minimize (Fig. 6a) and maximize (Fig. 6b) the differences between the models. The figures clearly indicate that the shallower layer (0—–0.35 m) is most significantly affected by the increase in P-wave velocity with a change of more than 50 %, due to compaction. It is noteworthy that variations in V_p are observed even beyond 0.5 m, with values exceeding 40 % for the HC treatment and approximately 20 % for LC compared to uncompacted soil.

4.3. Multichannel analysis of surface waves

Fig. 7 presents six different Vs profiles obtained from the inversion of dispersion curves. Upon analyzing the dispersion curves themselves, it is observed that for NC, the phase velocity trend is monotonically decreasing from 100 m s^{-1} at lower frequencies down to 80 m s^{-1} at frequencies exceeding 100 Hz. Conversely, as the surface compaction increases, the dispersion curves exhibit a curvature indicating higher phase velocities at higher frequencies. In general, the greater the degree of compaction, the greater the phase velocities, ranging from 110 − 90 m s^{-1} (i.e. LC) to 125–100 m s^{-1} (i.e. HC).

The described trend is also reflected by the V_s profiles after inversion. Considering the discretization of the model space into three layers, the higher shear-wave velocities were generally observed in deepest layer, located at a depth between 0.80 and 1.0 m, with values ranging between 125 and 150 m s^{-1}. The middle layer showed little variability among the three compaction levels with velocities ranging between 90 and 105 m s^{-1}, starting at approximately 0.20 m depth. Notably, the behavior of the top layer is of particular interest: the NC treatment showed lower velocities, averaging around 75 m s^{-1}. Conversely in the compacted treatments, the top layer exhibits higher velocities compared to the layer below, averaging at 107 m s^{-1} for LC and exceeding 140 m s^{-1} for HC. This is another indication illustrating the expectation that soil compaction influences mechanical properties at different depths.

4.4. Relationship between soil properties and seismic geophysical values

Seismic velocities demonstrate highly significant correlations with soil properties (Fig. 8). As expected, the V_p waves exhibit positive correlation with soil water content, either gravimetric ($r = 0.75$, $p < 0.01$) and volumetric ($r = 0.82$, $p < 0.01$). Additionally, a significant positive correlation is also found with soil bulk density ($r = 0.67$, $p < 0.01$) and penetration resistance ($r = 0.65$, $p < 0.01$). Similarly, positive correlations are found between V_s and bulk density ($r = 0.63$, $p < 0.01$), and between V_s and water content ($r = 0.7$ and $r = 0.63$ for volumetric and gravimetric respectively, $p < 0.01$).

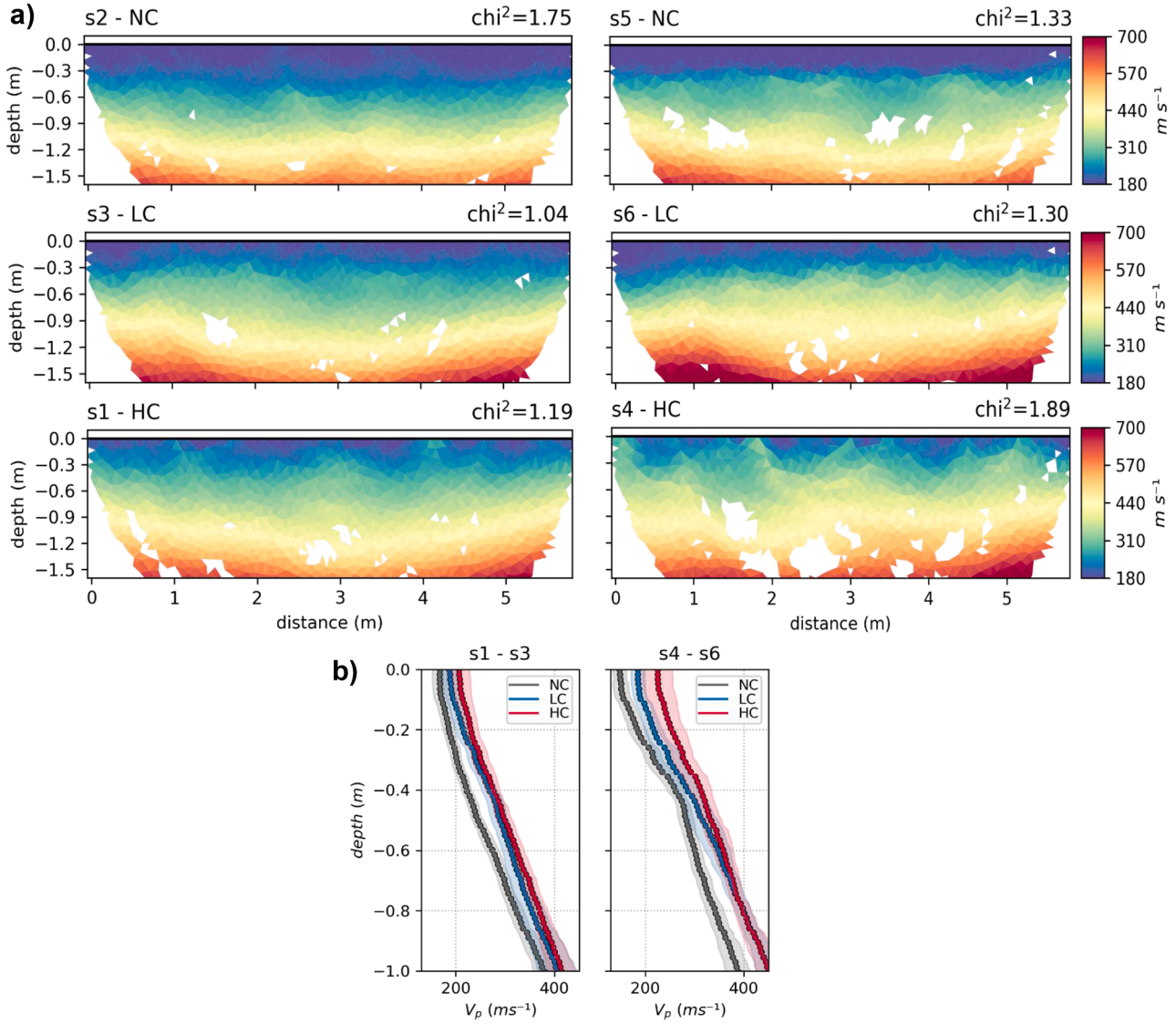

Fig. 5.

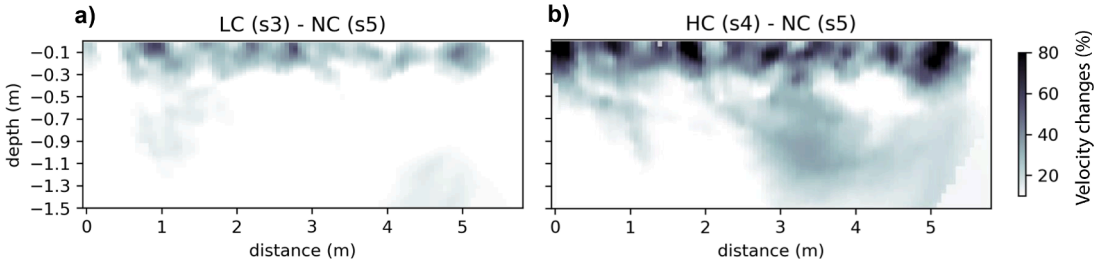

Fig. 6.

A backward multiple regression analysis was conducted to identify the ability of seismic wave methodology to determine the variability in soil bulk density. The results reported in Table 2 show that both V_p and V_s are selected together with GWC as significant predictors ($p < 0.05$) of soil bulk density. Their combination is in fact useful to explain 53 % of total soil bulk density variability. Contrarily, texture seems not useful to BD estimation. On the other hand, penetration resistance instead of seismic waves methodology is selected as significant predictor of BD only when associated with measures of ground truth gravimetric water content; in this case the explained BD variability is no more than 43 %.

5. Discussions

Both qualitative inspection of the subsurface geophysical models and quantitative analysis consistently show differences between the treatments under comparison.

Initially, we utilized soil bulk density as an indicator of the state of compaction and compared it with the seismic response. From a

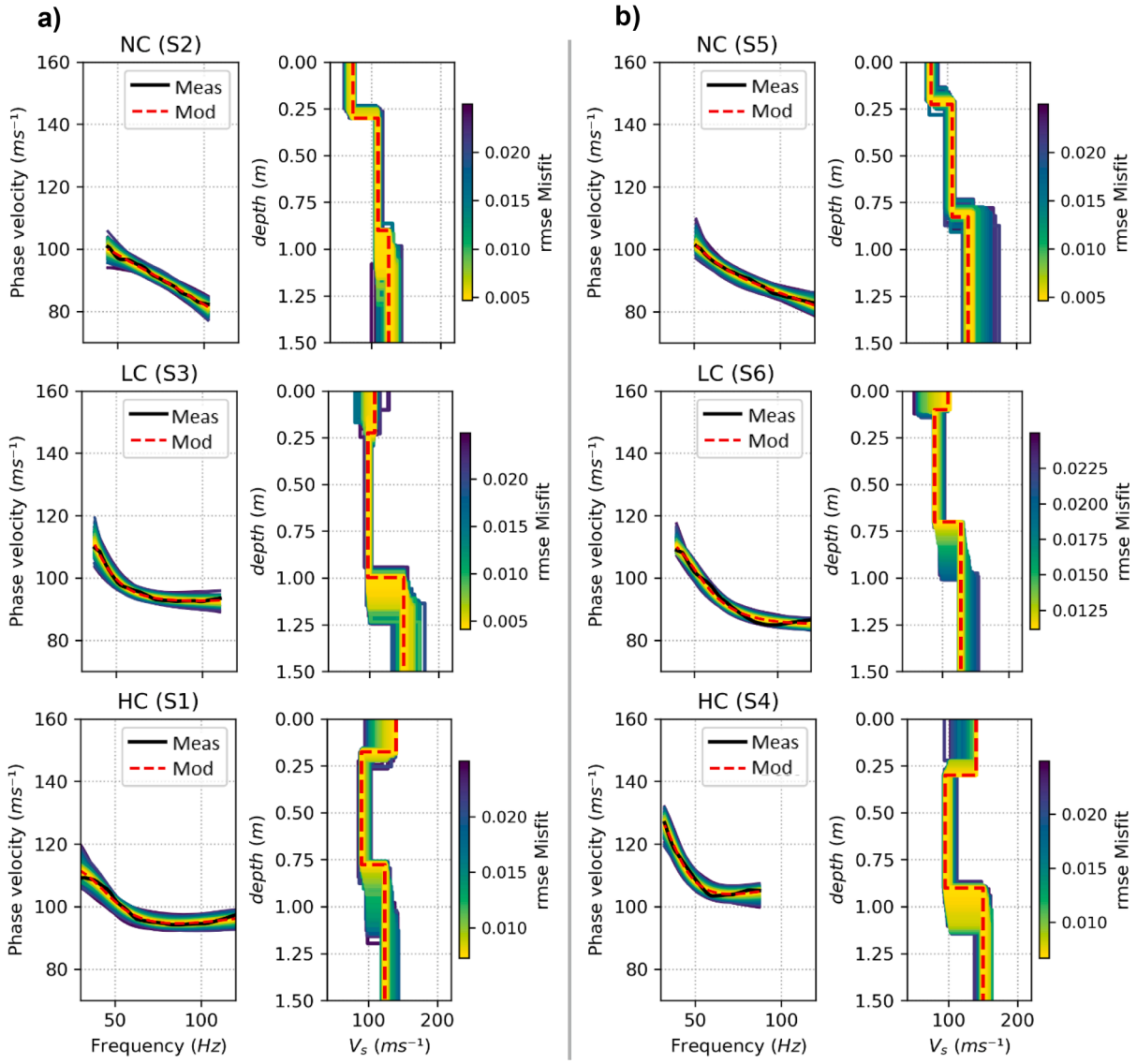

Fig. 7.

geophysical standpoint, a well-structured soil with lower BD than a compaction −degraded, hampers efficient propagation of seismic wave within the medium (Corapcioglu, 1991), establishing a direct relationship between BD and seismic propagation velocity (r = 0.69 and 0.63 for V_p and V_s respectively).

Although the differences between treatments were not statistically significant in terms of water content, a higher VWC can be appreciated in the first 0.4 m in compacted soil than in non-compacted (Fig. 4), as widely reported in the literature (e.g., Romero-Ruiz et al., 2022). Also notable is the change in the distribution of VWC and GWV along the soil profile, which generally shows an increasing trend with depth, uniform between treatments. This fact can be explained by the superficial influence of the experimental compaction, which mainly affected the first 0.4 m of soil.

Similarly, besides the known variability of these soils' properties (Piccoli et al., 2019; Sartori et al., 2022), compacted plots showed higher PR strengths than non-compacted plots in the shallowest portion (first 0.3 m depth), a phenomenon also widely recognized (e.g., Benevenute et al., 2020; Hamza and Anderson, 2005; Schjønning et al., 2015). All depth profiles of the described variables, including seismic, increase with increasing levels of experimental compaction (from NC to LC to HC).

Soils are complex, multiphase, composite, and physically discontinuous materials, making it challenging to accurately describe their mechanical behavior. Although linear elastic constitutive models are just an approximation of the real world (Boaga et al., 2021), many seismic techniques are based on elasticity theory due to the low strain levels involved. In our study, the SRT and MASW rely on linear elastic assumptions. Regarding P-wave SRT, the tomograms obtained from the inversion process revealed the spatial impact of compaction in the depth dimension covered by the survey length. Consistently with Ren et al. (2019), we observe that the influence of tractor tire pressure was concentrated in the top 0.4 m (>80 % V_p), with heterogeneity extending to greater depths and resulting in 20–40 % increases in V_p compared to uncompacted bare soil. We can probably assume that a percentage of seismic velocity variation is due to the capillary forces distribution arising during experimental compaction, as known from Solazzi et al. (2021). However, the water contents are similar for all treatments and therefore the capillary forces should also be similar, making us inclined to attribute the differences to compaction.

SRT is advantageous because it allows for the determination of a 2D velocity model of the subsoil based solely on the first-arrival time of the seismic energy, completely ignoring the phase and amplitude of the signal. However, the fundamental assumption behind SRT is that seismic

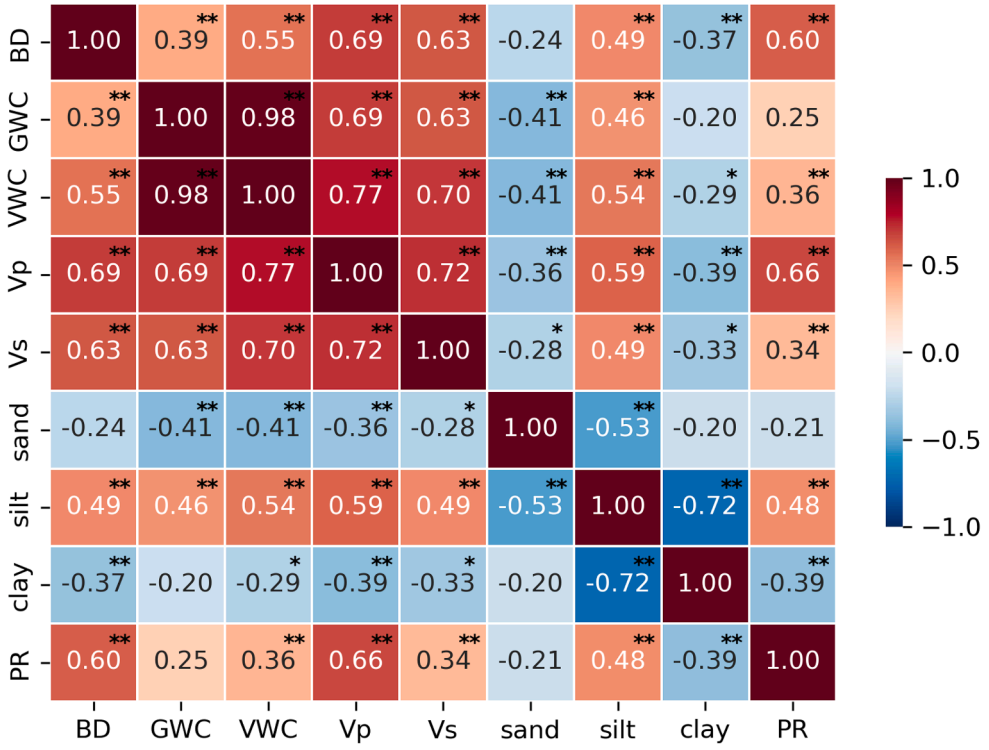

Fig. 8.

Table 2
Multiple linear regression analysis used to predict ground-truth soil bulk density by using inferential measures (seismic waves, penetration resistance) or penetration resistance, gravimetric water content (GWC) and inherent soil texture properties. Both unstandardized and standardized (in brackets) regression coefficients ($p < 0.05$) are reported.

		Regression coefficients						
	Intercept	**Sand (%)**	**Clay (%)**	**GWC (kg kg^{-1})**	**V_p (m/s)**	**V_s (m/s)**	**R^2**	**p-value**
BD	1.08	–	–	−0.30 (−0.59)	0.001 (0.65)	0.002 (0.33)	0.53	$p < 0.001$
	Intercept	**Sand (%)**	**Clay (%)**	**GWC (m3/m^{-3}(−|-))**	**PR (MPa)**		**R^2**	**p-value**
BD	1.27	–	–	0.51 (0.26)	0.095 (0.54)		0.43	$p < 0.001$

velocity predominantly increases with depth. Therefore, SRT is not capable of identifying velocity inversions with depth (Crutchley and Kopp, 2018; Green, 1974), which is also the case in our study. As a result, both the 2D models and the velocity profiles shown in Fig. 5 exhibit a general increase in velocity with depth, but also an increase in the range of velocities at the same depth compared with increasing degree of compaction, with the most pronounced effect at the shallowest depth range (0——0.35 m, Fig. 6). This phenomenon is well observed from the inversion ratios, from which it can also be deduced that soil deformation caused by machinery likely propagates to depths greater than 0.50 m.

On the other hand, surface wave methods (MASW in our case), although requiring slightly more complex data processing, provide results that are specifically related to the solid matrix. These methods use the information embedded in frequency-dependent high-amplitude surface waves, which can be easily recognized and generated during the same p-wave SRT survey, to estimate shear wave velocities. The inverted shear wave velocities varied vertically with the level of compaction, and they were found significantly correlated with proxies of soil compaction and densification.

The inversion of the dispersion curves (Fig. 7) revealed a "velocity inversion" phenomenon characterized by a soil layer with lower velocity than the overlying layer. This inversion was observed between the first two layers in both the HC and LC treatments, which were not visualized by the SRT method. The modelled velocities for the first 0.20 m in HC plots were on average 30 % higher than LC and more than 60 % higher than those in NC. This demonstrates the capability of the MASW method to effectively detect differences in soil properties which are here presumably related to different degrees of soil compaction. Nevertheless, during the inversion phase it was necessary to define *a priori* (i.e., from ground-truth and/or literature) a layered model space with ranges of thickness, V_s, V_p, density and Poisson's ratio in which to search for the solution. However, with more frequent use of the MASW technique in different sites and conditions, it is possible to populate a universal database enabling the standardization of search ranges without the need for site-specific calibration.

Finally, the multiple regression analysis (Tab. 2) provided valuable insights into the potential of seismic methods for estimating bulk density. The combination of shear wave velocity and compressional wave velocity, associated with soil water content determination, was able to explain 53 % of the observed variability in bulk density. In comparison, the traditional parameters such as penetration resistance and soil moisture could only account for 43 % of the variability. Texture did not appear to be useful for estimating BD, probably due to the uniform soil texture conditions within the experimental field. Although our analysis between measured and estimated soil compaction showed good

relationships, and the plots were all located in the same small area, care must be taken when extending these results to wider areas, where other external factors (e.g., variation in texture, soil cover, etc.) could lead to differences in BD compared to those estimated by seismic models.

6. Conclusions

In this work, we adapted active seismic techniques to the pedological scale and explored their ability to detect the compaction phenomenon. We specifically explored the sensitivity of these techniques in assessing various degrees of shallow soil compaction in a field environment.

Both the SRT and MASW methods clearly revealed significant differences of compressional (V_p) and shear (V_s) wave velocities, among different levels of compaction with almost identical soil textural properties. The SRT workflow, which has been long-established, primarily highlighted the surface compaction, especially in relative terms (Fig. 6). In contrast, the surface wave approach, although more complex and user's experience-dependent, was able to identify velocity inversions in the top layers, thus proving a much superior technique for this type of study.

The results obtained from the geophysical techniques were correlated and validated with those obtained from traditional direct soil measurements (i.e. bulk density, volumetric water content, texture and penetration resistance).

The combined geophysical approach presented in this paper offers several advantages over traditional measurements. Firstly, it is a non-intrusive method that allows to collect a large amount of data in a relatively short time. Additionally, simultaneous recording of V_p and V_s with the same instruments provides a cost-effective two-in-one solution. However, it is important to note that accurate data analysis and inversion are crucial for obtaining reliable results. The success of the method relies on performing these steps diligently. Future developments of this work may involve the development of a system capable of mapping large areas in a short time. This could involve the use of geophones mounted on land streamers connected to motor vehicles and dragged over hectares of land. Furthermore, the development of software that allows for rapid semi-automation of data processing, both for P-wave and S-wave analysis, would significantly streamline the workflow.

CRediT authorship contribution statement

Alberto Carrera: Writing – review & editing, Writing – original draft, Methodology, Investigation, Data curation, Conceptualization. **Ilaria Barone:** Writing – review & editing, Supervision, Methodology. **Mirko Pavoni:** Writing – review & editing, Investigation. **Jacopo Boaga:** Writing – review & editing, Supervision, Methodology. **Nicola Dal Ferro:** Writing – review & editing, Data curation. **Giorgio Cassiani:** Writing – review & editing, Supervision, Methodology. **Francesco Morari:** Writing – review & editing, Validation, Supervision, Funding acquisition.

Declaration of competing interest

The authors declare that they have no known competing financial interests or personal relationships that could have appeared to influence the work reported in this paper.

Data availability

Data will be made available on request.

Acknowledgments

The research leading to these results has received funding from the European Union's Horizon 2020 and MIPAAF - Italian Ministry of agriculture food and forestry policies research and innovation programme (grant agreement no 862665 ICT-AGRI-FOOD, SoCoRisk project). We are grateful to associate editor Haly Neely, reviewer Ellen Van De Vijver, and the other anonymous reviewers for their contribution on the earlier version of the manuscript.

REFERENCES

Aki, K., Richards, P.G., 1980. Quantitative seismology : theory and methods. W.H. Freeman.

Alaoui, A., Diserens, E., 2018. Mapping soil compaction – A review. Curr. Opin. Environ. Sci. Heal. 5, 60–66. https://doi.org/10.1016/j.coesh.2018.05.003.

Ammon, C.J., Velasco, A.A., Lay, T., Wallace, T.C., 2021. Elasticity and seismic waves, in: Foundations of Modern Global Seismology. Academic Press, pp. 305–338. 10.1016/b978-0-12-815679-7.00019-7.

Barone, I., Boaga, J., Carrera, A., Flores-Orozco, A., Cassiani, G., 2021. Tackling Lateral Variability Using Surface Waves: A Tomography-Like Approach. Surv. Geophys. 42, 317–338. https://doi.org/10.1007/s10712-021-09631-x.

Barone, I., Cassiani, G.G., Ourabah, A., Boaga, J., Pavoni, M., Deiana, R., 2023. Integrating controlled-source and ambient noise seismic measures for archaeological prospection: the Scrovegni Chapel case. Geophys. J. Int. 232, 1944–1956. https://doi.org/10.1093/gji/ggac432.

Barone, I., Cassiani, G., Ourabah, A., Boaga, J., Pavoni, M., Deiana, R., 2022. Surface wave tomography using dense 3D data around the Scrovegni Chapel in Padua, Italy. Sci. Reports 2022 121 12, 1–8. 10.1038/s41598-022-16061-1.

Benevenute, P.A.N., de Morais, E.G., Souza, A.A., Vasques, I.C.F., Cardoso, D.P., Sales, F. R., Severiano, E.C., Homem, B.G.C., Casagrande, D.R., Silva, B.M., 2020. Penetration resistance: An effective indicator for monitoring soil compaction in pastures. Ecol. Indic. 117 https://doi.org/10.1016/j.ecolind.2020.106647.

Besson, A., Séger, M., Giot, G., Cousin, I., 2013. Identifying the characteristic scales of soil structural recovery after compaction from three in-field methods of monitoring. Geoderma 204–205, 130–139. https://doi.org/10.1016/j.geoderma.2013.04.010.

Bittelli, M., Andrenelli, M.C.C., Simonetti, G., Pellegrini, S., Artioli, G., Piccoli, I., Morari, F., 2019. Shall we abandon sedimentation methods for particle size analysis in soils? Soil Tillage Res. 185, 36–46. https://doi.org/10.1016/j.still.2018.08.018.

Blanchy, G., Watts, C.W., Ashton, R.W., Webster, C.P., Hawkesford, M.J., Whalley, W.R., Binley, A., 2020. Accounting for heterogeneity in the θ–σ relationship: Application to wheat phenotyping using EMI. Vadose Zo. J. 19 https://doi.org/10.1002/vzj2.20037.

Blazevic, L.A., Bodet, L., Pasquet, S., Linde, N., Jougnot, D., Longuevergne, L., 2020. Time-lapse seismic and electrical monitoring of the vadose zone during a controlled infiltration experiment at the ploemeur hydrological observatory. France. Water (switzerland) 12. https://doi.org/10.3390/W12051230.

Boaga, J., Vignoli, G., Cassiani, G., 2011. Shear wave profiles from surface wave inversion: the impact of uncertainty on seismic site response analysis. J. Geophys. Eng 8, 162–174. https://doi.org/10.1088/1742-2132/8/2/004.

Boaga, J., Cassiani, G., Strobbia, C.L., Vignoli, G., 2013. Mode misidentification in Rayleigh waves: Ellipticity as a cause and a cure. Geophysics 78. https://doi.org/10.1190/GEO2012-0194.1.

Boaga, J., Vignoli, G., Deiana, R., Cassiani, G., 2014. The influence of subsoil structure and acquisition parameters in MASW mode mis-identification. J. Environ. Eng. Geophys. 19, 87–99. https://doi.org/10.2113/JEEG19.2.87.

Boaga, J., Barone, I., Deidda, G.P., Cassiani, G., Strobbia, C., 2021. Multi-drive level Vibroseis test to evaluate the non-linear response of soft soils. Soil Dyn. Earthq. Eng. 149, 106861 https://doi.org/10.1016/J.SOILDYN.2021.106861.

Born, M., Wolf, E., Hecht, E., 1959. Principles of Optics: Electromagnetic Theory of Propagation, Interference and Diffraction of Light. Pergamon Press. Pergamon Press. DOI 10 (1063/1), 1325200.

Bronick, C.J., Lal, R., 2004. Soil Structure and Management: a Review. https://doi.org/10.1016/j.geoderma.2004.03.005.

Carrera, A., Longo, M., Piccoli, I., Mary, B., Cassiani, G., Morari, F., 2022. Electro-Magnetic Geophysical Dynamics under Conservation and Conventional Farming. Remote Sens. 14, 6243. https://doi.org/10.3390/rs14246243.

Cassiani, G., Boaga, J., Vanella, D., Perri, M.T., Consoli, S., 2015. Monitoring and modelling of soil-plant interactions: The joint use of ERT, sap flow and eddy covariance data to characterize the volume of an orange tree root zone. Hydrol. Earth Syst. Sci. 19, 2213–2225. https://doi.org/10.5194/hess-19-2213-2015.

Cho, H.M., Baag, C.E., Lee, J.M., Moon, W.M., Jung, H., Kim, K.Y., Asudeh, I., 2006. Crustal velocity structure across the southern Korean Peninsula from seismic refraction survey. Geophys. Res. Lett. 33 https://doi.org/10.1029/2005GL025145.

Coppola, A., Gerke, H.H., Comegna, A., Basile, A., Comegna, V., 2012. Dual-permeability model for flow in shrinking soil with dominant horizontal deformation. Water Resour. Res. 48 https://doi.org/10.1029/2011WR011376.

Corapcioglu, M.Y., 1991. Wave propagation in porous media - a review. Transp. Process. Porous Media 373–469. https://doi.org/10.1007/978-94-011-3628-0_8.

Crutchley, G.J., Kopp, H., 2018. Reflection and Refraction Seismic Methods, in: Springer Geology. Springer, pp. 43–62. https://doi.org/10.1007/978-3-319-57852-1_4.

Darijani, M., Farquharson, C.G., Lelièvre, P.G., 2020. Clustering and constrained inversion of seismic refraction and gravity data for overburden stripping: Application to uranium exploration in the Athabasca Basin, Canada. Geophysics 85, B133–B146. 10.1190/GEO2019-0525.1.

Dexter, A.R., 1988. Advances in characterization of soil structure. Soil Tillage Res. 11, 199–238. https://doi.org/10.1016/0167-1987(88)90002-5.

Donohue, S., Forristal, D., Donohue, L.A., 2013. Detection of soil compaction using seismic surface waves. Soil Tillage Res. 128, 54–60. https://doi.org/10.1016/j.still.2012.11.001.
Doolittle, J.A., Brevik, E.C., 2014. The use of electromagnetic induction techniques in soils studies. Geoderma. https://doi.org/10.1016/j.geoderma.2014.01.027.
Everett, M.E., 2011. Near-surface applied geophysics, Near-Surface Applied Geophysics. Cambridge University Press. 10.1017/CBO9781139088435.
Fabiola, N., Giarola, B., Da Silva, A.P., Imhoff, S., Dexter, A.R., 2003. Contribution of natural soil compaction on hardsetting behavior. Geoderma 113, 95–108. https://doi.org/10.1016/S0016-7061(02)00333-6.
Fleisch, D., Kinnaman, L., 2015. A Student's Guide to Waves, Cambridge University Press. Cambridge University Press. 10.1017/CBO9781107294929.
Fomin, D.S., Yudina, A.V., Romanenko, K.A., Abrosimov, K.N., Karsanina, M.V., Gerke, K.M., 2023. Soil pore structure dynamics under steady-state wetting-drying cycle. Geoderma 432, 116401. https://doi.org/10.1016/J.GEODERMA.2023.116401.
Foti, S., Parolai, S., Albarello, D., Picozzi, M., 2011. Application of Surface-Wave Methods for Seismic Site Characterization. Surv. Geophys. 32, 777–825. https://doi.org/10.1007/S10712-011-9134-2/FIGURES/25.
Foti, S., Lai, C.G., Rix, G.J., Strobbia, C., 2014. Surface wave methods for near-surface site characterization. CRC Press.
Green, R., 1974. The seismic refraction method-a review. Geoexploration 12, 259–284. https://doi.org/10.1016/0016-7142(74)90015-5.
Grossman, R.B., Reinsch, T.G., 2018. The Solid Phase: Bulk Density and Linear Extensibility. Methods Soil Anal. Part 4 Phys. Methods 201–228. https://doi.org/10.2136/SSSABOOKSER5.4.C9.
Günther, T., Rücker, C., Spitzer, K., 2006. Three-dimensional modelling and inversion of dc resistivity data incorporating topography - II. Inversion. Geophys. J. Int. 166, 506–517. https://doi.org/10.1111/J.1365-246X.2006.03011.X/2/166-2-506-TBL003.JPEG.
Gürsoy, S., 2021. Soil Compaction Due to Increased Machinery Intensity in Agricultural Production: Its Main Causes, Effects and Management, in: Technology in Agriculture. IntechOpen. 10.5772/intechopen.98564.
Hamza, M.A., Anderson, W.K., 2005. Soil compaction in cropping systems: A review of the nature, causes and possible solutions. Soil Tillage Res. 82, 121–145. https://doi.org/10.1016/J.STILL.2004.08.009.
Hansen, P.C., 2000. The L-Curve and its Use in the Numerical Treatment of Inverse Problems. Comput. Inverse Probl. Electrocardiology, ed. P. Johnston. Adv. Comput. Bioeng. 4, 119–142.
Hanssens, D., Delefortrie, S., Bobe, C., Hermans, T., De Smedt, P., 2019. Improving the reliability of soil EC-mapping: Robust apparent electrical conductivity (rECa) estimation in ground-based frequency domain electromagnetics. Geoderma 337, 1155–1163. https://doi.org/10.1016/j.geoderma.2018.11.030.
Hara, A., Ohta, T., Niwa, M., Tanaka, S., Banno, T., 1974. Shear Modulus and Shear Strength of Cohesive Soils. Soils Found. 14, 1–12. https://doi.org/10.3208/sandf1972.14.3_1.
Islam, M.M., Meerschman, E., Saey, T., De Smedt, P., Van De Vijver, E., Delefortrie, S., Van Meirvenne, M., 2014a. Characterizing Compaction Variability with an Electromagnetic Induction Sensor in a Puddled Paddy Rice Field. Soil Sci. Soc. Am. J. 78, 579–588. https://doi.org/10.2136/sssaj2013.07.0289.
Islam, M.M., Saey, T., De Smedt, P., Van De Vijver, E., Delefortrie, S., Van Meirvenne, M., 2014b. Modeling within field variation of the compaction layer in a paddy rice field using a proximal soil sensing system. Soil Use Manag. 30, 99–108. https://doi.org/10.1111/sum.12098.
Johnson, E.C., Bailey, A.C., 2002. Soil Compaction. Adv. Soil Dyn. 2, 155. https://doi.org/10.13031/2013.9452.
Jonard, F., Mahmoudzadeh, M., Roisin, C., Weihermüller, L., André, F., Minet, J., Vereecken, H., Lambot, S., 2013. Characterization of tillage effects on the spatial variation of soil properties using ground-penetrating radar and electromagnetic induction. Geoderma 207–208, 310–322. https://doi.org/10.1016/j.geoderma.2013.05.024.
Kearey, P., Brooks, M., 2002. An introduction to geophysical exploration. 2nd edition. An Introd. to Geophys. Explor. 2nd Ed. 262.
Keller, T., Colombi, T., Ruiz, S., Schymanski, S.J., Weisskopf, P., Koestel, J., Sommer, M., Stadelmann, V., Breitenstein, D., Kirchgessner, N., Walter, A., Or, D., 2021. Soil structure recovery following compaction: Short-term evolution of soil physical properties in a loamy soil. Soil Sci. Soc. Am. J. 85, 1002–1020. https://doi.org/10.1002/SAJ2.20240.
Keller, T., Carizzoni, M., Berisso, F.E., Stettler, M., Lamandé, M., 2013. Measuring the Dynamic Soil Response During Repeated Wheeling Using Seismic Methods. Vadose Zo. J. 12, vzj2013.01.0033. 10.2136/vzj2013.01.0033.
Keller, T., Lamandé, M., Naderi-Boldaji, M., de Lima, R.P., 2021b. Soil Compaction Due to Agricultural Field Traffic: An Overview of Current Knowledge and Techniques for Compaction Quantification and Mapping, in: Advances in Understanding Soil Degradation. Springer, Cham, pp. 287–312. 10.1007/978-3-030-85682-3_13.
Keller, T., Lamandé, M., Naderi-Boldaji, M., Paiva, L.R., de, 2018. Approaches towards understanding soil compaction processes. Novel Methods and Results of Landscape Research in Europe, Central Asia and Siberia. 274–279.
Keller, T., Sandin, M., Colombi, T., Horn, R., Or, D., 2019. Historical increase in agricultural machinery weights enhanced soil stress levels and adversely affected soil functioning. Soil Tillage Res. 194, 104293 https://doi.org/10.1016/j.still.2019.104293.
Lehmann, B., 2007. Seismic traveltime tomography for engineering and exploration applications, ebook - Seismic traveltime tomography for engineering and exploration applications. Earthdoc. https://doi.org/10.3997/9789462820166.
Longo, M., Dal Ferro, N., Lazzaro, B., Morari, F., 2021. Trade-offs among ecosystem services advance the case for improved spatial targeting of agri-environmental measures. J. Environ. Manage. 285, 112131 https://doi.org/10.1016/j.jenvman.2021.112131.
Luu, K., 2021a. evodcinv: Inversion of dispersion curves using Evolutionary Algorithms. 10.5281/ZENODO.5785565.
Luu, K., 2021b. stochopy: Python library for stochastic numerical optimization. 10.5281/ZENODO.5717781.
Ma, Y.Z., Sobernheim, D., Garzon, J.R., 2016. Glossary for Unconventional Oil and Gas Resource Evaluation and Development. Unconv. Oil Gas Resour. Handb. Eval. Dev. 513–526 https://doi.org/10.1016/B978-0-12-802238-2.00019-5.
Mencaroni, M., Longo, M., Cardinali, A., Lazzaro, B., Zanin, G., Dal Ferro, N., Morari, F., 2023. Glyphosate and AMPA dynamics during the transition towards conservation agriculture: Drivers under shallow groundwater conditions. Soil Tillage Res. 229, 105659 https://doi.org/10.1016/J.STILL.2023.105659.
Morari, F., Castrignanò, A., Pagliarin, C., 2009. Application of multivariate geostatistics in delineating management zones within a gravelly vineyard using geo-electrical sensors. Comput. Electron. Agric. 68, 97–107. https://doi.org/10.1016/j.compag.2009.05.003.
Moser, T.J., 1991. Shortest path calculation of seismic rays. Geophysics 56, 59–67. https://doi.org/10.1190/1.1442958.
Moser, T., Nolet, G., the, R.S.-B. of, 1992, undefined, 1992. Ray bending revisited. pubs.geoscienceworld.org 82, 259–288.
Muñiz, E., Shaw, R.K., Gimenez, D., Williams, C.A., Kenny, L., 2016. Use of Ground-Penetrating Radar to Determine Depth to Compacted Layer in Soils Under Pasture. Springer, Cham, pp. 411–421. 10.1007/978-3-319-28295-4_26.
Nawaz, M.F., Bourrié, G., Trolard, F., 2012. Soil compaction impact and modelling. A Review. https://doi.org/10.1007/s13593-011-0071-8.
Park, C.B., Miller, R.D., Xia, J., 1999. Multichannel analysis of surface waves. Geophysics 64, 800–808. https://doi.org/10.1190/1.1444590.
Pasquet, S., Bodet, L., Bergamo, P., Guérin, R., Martin, R., Mourgues, R., Tournat, V., 2016. Small-Scale Seismic Monitoring of Varying Water Levels in Granular Media. Vadose Zo. J. 15, 1–14. https://doi.org/10.2136/vzj2015.11.0142.
Pelissier, M.A., 2007. 3p. On Elasticity of Porous Media by F. Gassmann, Zürich, 1951, in: Classics of Elastic Wave Theory. Society of Exploration Geophysicists, pp. 389–408. 10.1190/1.9781560801931.ch3p.
Piccoli, I., Furlan, L., Lazzaro, B., Morari, F., 2019. Examining conservation agriculture soil profiles: Outcomes from northeastern Italian silty soils combining indirect geophysical and direct assessment methods. Eur. J. Soil Sci. 71, 1064–1075. https://doi.org/10.1111/ejss.12861.
Raper, R.L., 2005. Agricultural traffic impacts on soil. J. Terramechanics 42, 259–280. https://doi.org/10.1016/J.JTERRA.2004.10.010.
Rayleigh, L., 1885. On waves propagated along the plane surface of an elastic solid. Proc. London Math. Soc. s1–17, 4–11. https://doi.org/10.1112/plms/s1-17.1.4.
Ren, L., D'Hose, T., Ruysschaert, G., De Pue, J., Meftah, R., Cnudde, V., Cornelis, W.M., 2019. Effects of soil wetness and tyre pressure on soil physical quality and maize growth by a slurry spreader system. Soil Tillage Res. 195, 104344 https://doi.org/10.1016/J.STILL.2019.104344.
Richart, F.E., HALL, J.R., Woods, R.D., 1970. Vibration of soils and foundation.
Romero-Ruiz, A., Linde, N., Baron, L., Breitenstein, D., Keller, T., Or, D., 2022. Lasting Effects of Soil Compaction on Soil Water Regime Confirmed by Geoelectrical Monitoring. Water Resour. Res. 58, e2021WR030696. 10.1029/2021WR030696.
Romero-Ruiz, A., Linde, N., Keller, T., Or, D., 2018. A Review of Geophysical Methods for Soil Structure Characterization. Rev. Geophys. https://doi.org/10.1029/2018RG000611.
Romero-Ruiz, A., Linde, N., Baron, L., Solazzi, S.G., Keller, T., Or, D., 2021. Seismic signatures reveal persistence of soil compaction. Vadose Zo. J. 20, e20140.
Rücker, C., Günther, T., Wagner, F.M., 2017. pyGIMLi: An open-source library for modelling and inversion in geophysics. Comput. Geosci. 109, 106–123. https://doi.org/10.1016/j.cageo.2017.07.011.
Samyn, K., Travelletti, J., Bitri, A., Grandjean, G., Malet, J.P., 2012. Characterization of a landslide geometry using 3D seismic refraction traveltime tomography: The La Valette landslide case history. J. Appl. Geophys. 86, 120–132. https://doi.org/10.1016/J.JAPPGEO.2012.07.014.
Sartori, F., Piccoli, I., Polese, R., Berti, A., 2022. Transition to Conservation Agriculture: How Tillage Intensity and Covering Affect Soil Physical Parameters 8, 213–222. https://doi.org/10.5194/soil-8-213-2022.
Schjønning, P., Akker, J.J.H. Van Den, Keller, T., 2015. Driver-Pressure-State-Impact-Response (DPSIR) Analysis and Risk Assessment for Soil Compaction d A European Perspective.
Schjønning, P., Lamandé, M., Thorsøe, M.H., 2019. Soil compaction - drivers, pressures, state, impacts and responses. DCA Rep.
Seladji, S., Cosenza, P., Tabbagh, A., Ranger, J., Richard, G., 2010. The effect of compaction on soil electrical resistivity: A laboratory investigation. Eur. J. Soil Sci. 61, 1043–1055. https://doi.org/10.1111/j.1365-2389.2010.01309.x.
Shin, H.C., Whalley, W.R., Attenborough, K., Taherzadeh, S., 2016. On the theory of Brutsaert about elastic wave speeds in unsaturated soils. Soil Tillage Res. 156, 155–165. https://doi.org/10.1016/J.STILL.2015.10.006.
Solazzi, S.G., Bodet, L., Holliger, K., Jougnot, D., 2021. Surface-Wave Dispersion in Partially Saturated Soils: The Role of Capillary Forces. J. Geophys. Res. Solid Earth 126. https://doi.org/10.1029/2021JB022074.
Telford, W.M., Geldart, L.P., Sheriff, R.E., 1990. Applied Geophysics. Appl. Geophys. https://doi.org/10.1017/CBO9781139167932.
Thomson, W.T., 1950. Transmission of elastic waves through a stratified solid medium. J. Appl. Phys. 21, 89–93. https://doi.org/10.1063/1.1699629.

Tokimatsu, K., Tamura, S., Kojima, H., 1992. Effects of Multiple Modes on Rayleigh Wave Dispersion Characteristics. J. Geotech. Eng. 118, 1529–1543. https://doi.org/10.1061/(ASCE)0733-9410(1992)118:10(1529).

Tselentis, G.A., Delis, G., 1998. Rapid assessment of S-wave profiles from the inversion of multichannel. Ann. Geophys. 41 https://doi.org/10.4401/ag-3788.

Uhlemann, S., Hagedorn, S., Dashwood, B., Maurer, H., Gunn, D., Dijkstra, T., Chambers, J., 2016. Landslide characterization using P- and S-wave seismic refraction tomography — The importance of elastic moduli. J. Appl. Geophys. 134, 64–76. https://doi.org/10.1016/J.JAPPGEO.2016.08.014.

Uyanik, O., 2010. Compressional and shear-wave velocity measurements in unconsolidated top-soil and comparison of the results. Int. J. Phys. Sci. 5, 1034–1039.

Vignoli, G., Cassiani, G., 2010. Identification of lateral discontinuities via multi-offset phase analysis of surface wave data. Geophys. Prospect. 58, 389–413. https://doi.org/10.1111/j.1365-2478.2009.00838.x.

Vignoli, G., Strobbia, C., Cassiani, G., Vermeer, P., 2011. Statistical multioffset phase analysis for surface-wave processing in laterally varying media. Geophysics 76, U1–U11. https://doi.org/10.1190/1.3542076.

Vignoli, G., Gervasio, I., Brancatelli, G., Boaga, J., Della Vedova, B., Cassiani, G., 2016. Frequency-dependent multi-offset phase analysis of surface waves: An example of high-resolution characterization of a riparian aquifer. Geophys. Prospect. 64, 102–111. https://doi.org/10.1111/1365-2478.12256.

Virtanen, P., Gommers, R., Oliphant, T.E., Haberland, M., Reddy, T., Cournapeau, D., Burovski, E., Peterson, P., Weckesser, W., Bright, J., van der Walt, S.J., Brett, M., Wilson, J., Millman, K.J., Mayorov, N., Nelson, A.R.J., Jones, E., Kern, R., Larson, E., Carey, C.J., Polat, İ., Feng, Y., Moore, E.W., VanderPlas, J., Laxalde, D., Perktold, J., Cimrman, R., Henriksen, I., Quintero, E.A., Harris, C.R., Archibald, A.M., Ribeiro, A. H., Pedregosa, F., van Mulbregt, P., Vijaykumar, A., Bardelli, A.P., Rothberg, A., Hilboll, A., Kloeckner, A., Scopatz, A., Lee, A., Rokem, A., Woods, C.N., Fulton, C., Masson, C., Häggström, C., Fitzgerald, C., Nicholson, D.A., Hagen, D.R., Pasechnik, D.V., Olivetti, E., Martin, E., Wieser, E., Silva, F., Lenders, F., Wilhelm, F., Young, G., Price, G.A., Ingold, G.L., Allen, G.E., Lee, G.R., Audren, H., Probst, I., Dietrich, J.P., Silterra, J., Webber, J.T., Slavič, J., Nothman, J., Buchner, J., Kulick, J., Schönberger, J.L., de Miranda Cardoso, J.V., Reimer, J., Harrington, J., Rodríguez, J.L.C., Nunez-Iglesias, J., Kuczynski, J., Tritz, K., Thoma, M., Newville, M., Kümmerer, M., Bolingbroke, M., Tartre, M., Pak, M., Smith, N.J., Nowaczyk, N., Shebanov, N., Pavlyk, O., Brodtkorb, P.A., Lee, P., McGibbon, R.T., Feldbauer, R., Lewis, S., Tygier, S., Sievert, S., Vigna, S., Peterson, S., More, S., Pudlik, T., Oshima, T., Pingel, T.J., Robitaille, T.P., Spura, T., Jones, T.R., Cera, T., Leslie, T., Zito, T., Krauss, T., Upadhyay, U., Halchenko, Y.O., Vázquez-Baeza, Y., 2020. SciPy 1.0: fundamental algorithms for scientific computing in Python. Nat. Methods 17, 261–272. https://doi.org/10.1038/s41592-019-0686-2.

Wagner, F.M., Uhlemann, S., 2021. An overview of multimethod imaging approaches in environmental geophysics. Adv. Geophys. 62, 1–72. https://doi.org/10.1016/bs.agph.2021.06.001.

White, D.J., 1989. Two-dimensional seismic refraction tomography. Geophysical Journal. https://doi.org/10.1111/j.1365-246X.1989.tb00498.x.

Woodward, M.J., 1992. Wave-equation tomography. Geophysics 57, 15–26. https://doi.org/10.1190/1.1443179.

WRB, I.W.G., 2014. World Reference Base for Soil Resources 2014. International Soil Classification System for Naming Soils and Creating Legends for Soil Maps, World Soil Resources Reports No. 106, FAO, Rome. FAO Rome, Italy.

Wright, P.M., 1981. Seismic Methods in Mineral Exploration. Econ. Geol. Seventy-Fifth Anniv. 853–860 https://doi.org/10.5382/AV75.27.

Xia, J., Miller, R.D., Park, C.B., 1999. Estimation of near-surface shear-wave velocity by inversion of Rayleigh waves. Geophysics 64, 691–700. https://doi.org/10.1190/1.1444578.

Zajícová, K., Chuman, T., 2019. Application of ground penetrating radar methods in soil studies: A review. Geoderma 343, 116–129. https://doi.org/10.1016/J.GEODERMA.2019.02.024.

Zelt, C.A., Sain, K., Naumenko, J.V., Sawyer, D.S., 2003. Assessment of crustal velocity models using seismic refraction and reflection tomography. Geophys. J. Int. 153, 609–626. https://doi.org/10.1046/J.1365-246X.2003.01919.X/3/153-3-609-FIG010.JPEG.

Zhang, S.X., Chan, L.S., 2003. Possible effects of misidentified mode number on Rayleigh wave inversion. J. Appl. Geophys. 53, 17–29. https://doi.org/10.1016/S0926-9851(03)00014-4.